https://doi.org/10.5194/egusphere-2023-2892
Preprint. Discussion started: 2 January 2024

Unlocking the Potential of Melting Calorimetry: A Field Protocol for Liquid Water Content Measurement in Snow

Riccardo Barella[1,*], Mathias Bavay[2], Francesca Carletti[2], Nicola Ciapponi[1], Valentina Premier[1], and Carlo Marin[1,*]

[1]Institute for Earth Observation, Eurac Research, Viale Druso, 1 - 39100 Bolzano, Italy
[2]WSL Institute for Snow and Avalanche Research SLF, Davos, 7260, Switzerland
[*]These authors contributed equally to this work.

Correspondence: carlo.marin@eurac.edu

Abstract. Melting calorimetry, a classic experiment conducted in high school chemistry laboratories using calorimeters made from coffee cups, holds untapped potential beyond its educational context. Despite the fact that in the past this technique has been successfully used to measure the liquid water content in snow, its widespread adoption was impeded as it is often unjustly associated with generating large measurement errors. This paper shows how this technique can be incorporated in a rigorous field protocol to measure the liquid water content in the snow providing also a quantification of the uncertainty associated to the measurements. The results presented here encourage the use of melting calorimetry in all cases where liquid water content of the snow has to be quantified.

1 Introduction

The presence of liquid water has a profound impact on the physical characteristics of snow, including advecting heat through preferential flow, thermal conductivity, density, and mechanical properties, consequently influencing its hydrological and stability responses (Techel and Pielmeier, 2011; Avanzi et al., 2017; Wever et al., 2016). Therefore, the precise measurement of liquid water content (LWC) within the snowpack assumes critical importance as it provides invaluable information to properly describe the current conditions of the snowpack and predict its evolution (Hirashima et al., 2019; Wever et al., 2014), and characterize the backscattering of radar signal e.g., (Gagliano et al., 2023; Marin et al., 2020).

Calorimetry is the scientific technique used to measure the heat energy transferred during a physical or chemical process, such as a reaction or a change in state. This is achieved by utilizing a calorimeter, a specialized device designed to accurately measure the heat exchanged between a system and its surroundings. It has emerged as a promising technique for LWC determination within the snowpack, e.g., (Yosida, 1960; Jones et al., 1983; Kawashima et al., 1998; Jones, 1979; Boyne and Fisk, 1987; Kinar and Pomeroy, 2015). To measure the LWC in snowpacks, calorimetry offers two distinct approaches based on the process involved: melting and freezing calorimeters. In a melting calorimeter, a snow sample is immersed in hot water. This results in the transition of the solid portion of the sample to a liquid phase, and the heating of the melted ice portion and of the LWC to the equilibrium temperature. The measurement of the energy required for this transition is directly related to the amount of ice present in the snow sample. Consequently, the LWC can be derived as the difference between the mass or

https://doi.org/10.5194/egusphere-2023-2892
Preprint. Discussion started: 2 January 2024

Table 1. List of Symbols

SYMBOL	Definition
θ_w	Snow Liquid Water Content expressed as percentage of liquid water for snow volume
V_s	Volume of the snow sample
M_s	Mass of the snow sample
M_i	Mass of the ice sample
M_w, M_o	Mass of the melting and of the freezing agent
R	Ratio between M_w and M_s
E	Calorimetric constant expressed in equivalent water mass
T_w, T_o	Hot water and freezing agent initial temperature
T_f	Final temperature of the system at the end of the experiment
M_{cal}	Calorimeter internal wall mass
C	Water specific heat i.e., 4.2×10^3 J kg^{-1}K^{-1}
C_i	Ice heat capacity i.e., 2.09×10^3 J kg^{-1}K^{-1}
C_o	Freezing agent specific heat. In the case of using silicone oil, C_o is 1.83×10^3 J kg^{-1}K^{-1} at $-10°C$.
C_{cal}	Calorimeter internal wall specific heat
L	Latent heat of ice fusion i.e., 3.34×10^5 J kg^{-1}
ρ_w	Water density i.e., 1000 kg m^{-3}
σ_{θ_w}	Uncertainty associated to the LWC measurement
$\sigma_{M_w}, \sigma_{M_w}$	Uncertainty associated to the mass of melting and freezing agent
σ_{M_s}	Uncertainty associated to the mass of the snow sample
$\sigma_{T_w}, \sigma_{T_o}$	Uncertainty associated to the measure of the melting and freezing agent
σ_{T_f}	Uncertainty associated to the final temperature of the system
σ_{V_s}	Uncertainty associated to the volume of the snow sample
σ_E	Uncertainty associated to the calorimetric constant

the volume of the sample and the ice content. On the contrary, a freezing calorimeter involves immersing a snow sample in a freezing agent such as cooled silicon oil that induces the transition of any liquid water in the sample to a solid phase, and the cooling of the ice fraction and of the freezed LWC to the equilibrium temperature. The measurement of the energy required for this transition is directly related to the amount of LWC present in the snow sample.

The selection of the most suitable approach for implementing calorimetry to measure LWC demands consideration of both field usage and the accuracy of the obtained results. Firstly, it becomes evident that the practical handling of these methods significantly varies. Specifically, the usage of freezing calorimeter presents several challenges. This calorimeter requires the use of a freezing agent such as silicone oils or toluene, which possess characteristics that make them less desirable for use. For instance, these agents may be toxic and pose difficulties in terms of proper disposal and clean of the instruments after use. Due

https://doi.org/10.5194/egusphere-2023-2892
Preprint. Discussion started: 2 January 2024

to the variability in the physical composition of the freezing agent caused the different in its preparation, its specific heat has to be retrieved through a dedicated analysis every time a new agent is used.

Furthermore, operating a freezing calorimeter poses challenges associated with maintaining the freezing agent within a temperature range of -50 to $-20°C$. This task is complicated by thermal losses and operational difficulties encountered in cooling down the active agent on the field. Additionally, active monitoring of temperature changes is required throughout the experiment, lasting at least 15 minutes (Fisk, 1986), to ensure complete freezing of the LWC and the system reaching thermal equilibrium. During this period, thermal losses can be substantial, introducing significant uncertainties. In melting calorimetry, keeping the melting agent warm in a cold environment remains an issue. However, this can be mitigated by using a portable stove to raise water temperature. In contrast to freezing calorimetry, a larger mass of water needs to be melted, requiring a considerable amount of energy. Despite this, the process, with proper mixing, can achieve thermal equilibrium quickly, resulting in fewer potential thermal losses through the calorimeter. This enhances the overall efficiency of the experiment compared to a freezing calorimeter.

Interestingly, researchers and users of the freezing calorimeter driven by the recognized difficulties associated with operating this instrument (Boyne and Fisk, 1987), have developed and employed alternative methods, such as the dilution method (Fisk, 1986), to mitigate some of these challenges. Surprisingly, little effort has been directed towards a practical comparison between freezing and melting calorimeters for measuring LWC (Linlor, 1975). This is mainly due to the common perception that melting calorimeters are prone to producing large errors. Indeed, in the study conducted by Colbeck (1978), several measuring techniques including the freezing and melting calorimeter were compared within a theoretical framework of propagation of the uncertainty. The primary objective was to determine the measuring methodology that would result in lower uncertainty when deriving the water saturation and porosity. The analysis revealed that the uncertainty is propagating in a larger quantity when starting from a measurement of ice volume i.e., utilizing the melting calorimeter compared to starting from a measurement of water volume i.e., employing the freezing calorimeter. Based on this analysis, assuming that the relative uncertainty in measuring the ice volume is similar or greater than that in measuring the water volume, the freezing calorimeter was deemed preferable over the melting calorimeter. However, the study provided only an intuitive explanation to support this assumption, suggesting that freezing a smaller amount of water leads to a reduced error compared to melting a larger amount of snow. This nonetheless overlooks the practical challenges associated with freezing a small amount of water within a snow sample under real-world conditions, as discussed previously. Even after the rigorous uncertainty propagation analysis of the melting calorimeter performed by Kawashima et al. (1998), which demonstrated an uncertainty comparable to that of the freezing calorimeter, the melting calorimeter did not experience widespread adaptation.

In this paper, we aim to compare the melting and freezing calorimetry techniques, focusing on their applicability for measurements in remote areas. Our findings indicate that the results obtained using the melting calorimeter are still accurate enough for an accurate analysis of LWC offering at the same time notable practical advantages. To support our claims, we have thoroughly examined and propagated uncertainties, encompassing not only instrumental factors but also variations arising from the operational procedures and environmental conditions. As a result, we have devised a field protocol that effectively minimizes these uncertainties. The protocol includes specific instructions on the amount of hot water to be used, its temperature,

https://doi.org/10.5194/egusphere-2023-2892
Preprint. Discussion started: 2 January 2024

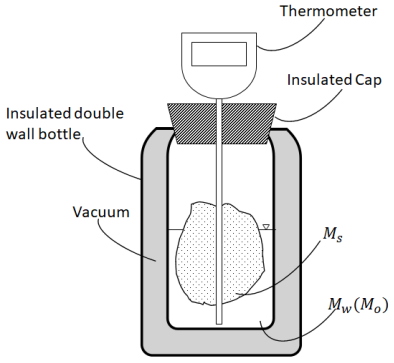

Figure 1. The figure illustrates a cross-section of the calorimeter, depicting a schematic representation of its components. In detail it is possible to notice the double wall insulated bottle and the vacuum in between the walls, a snow sample (M_s) immersed in the melting (M_w) or freezing agent (M_o). For convenience, the thermometer is embedded within the insulated cap of the system.

the size of the calorimeter, the masses involved, and other crucial details for controlling the uncertainty during the experiment replication. This protocol was applied in two different test sites in Italy and Switzerland by two different research groups with different melting calorimeters. The results, compared to independent measurements of dielectric constant of the snow, show how the application of the proposed protocol to the melting calorimeteric measurements is able to properly track the wet front penetration inside the snowpack in an accurate way.

2 Formulation of Melting and Freezing Calorimetry

The calorimeter experiment is formulated as an energy budget problem. Each term in the energy budget associated with a change in temperature depends on the mass involved, their specific heat, and the temperature difference. Conversely, terms related to phase transitions are determined by the mass involved and the latent heat. Before dealing with the computation of the energy balance, some practical considerations on the setup and measurement operations will be provided.

The setup for calorimetry used to measure LWC in snow involves three essential instruments: i) a specialized instrument known as a calorimeter (see Fig. 1), ii) a scale, and iii) a thermometer. The calorimeter is designed as an insulated container to maintain a given temperature and create an adiabatic environment, ensuring ideal heat exchange between the snow sample and the melting or freezing agent. The thermometer is generally already part of the calorimeter. It is inserted into the insulation cap of the calorimeter, with particular attention of introduce any points for heat exchanges, and is used to monitor temperature changes during the experiment.

From a practical point of view, the calorimetry experiment starts with the placement of a precisely measured mass of either melting agent (M_w) or freezing agent (M_o) into the insulated container. Commonly used melting agent is hot water, whereas the most used freezing agent is silicone oils. The initial temperature of the melting agent ($T_w \gg 0°C$) or the freezing agent ($T_o \ll 0°C$) is recorded. Subsequently, a snow sample of mass M_s and volume V_s is added to the calorimeter. The resulting

https://doi.org/10.5194/egusphere-2023-2892
Preprint. Discussion started: 2 January 2024

mixture is stirred to facilitate rapid mixing and efficient heat transfer. During this process, the temperature of the mixture is monitored until it reaches equilibrium (T_f), indicating the completion of the heat exchange between the snow sample and the agent. Minimizing the duration of these steps is essential to maintain the assumption of an adiabatic system (Kawashima et al., 1998). Any potential losses of the calorimeter, which may be large in the freezing calorimeter giving the low temperature of operation, must be accounted for in the analysis e.g., monitoring the temperature for long time (Jones et al., 1983). During the calorimetric experiment, heat exchange occurs not only between the snow sample and the fluid but also with the calorimeter walls. This additional heat exchange must be considered in the calculation by adding an extra term to the water mass, denoted as calorimeter constant E (Jones et al., 1983; Fasani et al., 2023). All these quantities are then used to calculate the heat exchanged during the process, allowing for an estimation of the liquid water content (θ_w) within the snowpack. As we progress with the paper, when we discuss LWC, we will be specifically referring to the volumetric LWC, which is a measure defined as the ratio of the volume of LWC to the volume of the snow sample.

In detail, in the melting calorimeter, the energy introduced by the hot water $Q_{hot;water}$ and the calorimeter's internal wall $Q_{Container}$ must balance with the sum of energy terms for the sinks. These include the heat needed for melting the ice content $Q_{ice;melt}$, the heat required to bring the melted ice and the liquid water already present in the snow to the equilibrium temperature $Q_{melted;ice}$ and Q_{LWC}. In Eq.(1) is shown the energy balance equation, detailing the different terms of the equations

$$\underbrace{Q_{hot\ water}}_{M_h^M C(T_f - T_w)} + \underbrace{Q_{Container}}_{M_c C_c (T_f - T_w)} + \underbrace{Q_{ice\ melting}}_{LM_i} + \underbrace{Q_{melted\ ice}}_{M_i C (T_f - T_s)} + \underbrace{Q_{LWC}}_{M_{W_{LWC}} C (T_f - T_s)} = 0 \tag{1}$$

Where, C and L represent the specific heat of water (4.2×10^3 J kg^{-1}K^{-1}) and the latent heat of fusion of ice (3.34×10^5 J kg^{-1}), respectively, ρ_w is the density of water i.e., 1000 kg m^{-3} and E is the calorimeter constant expressed in g. T_s is the temperature of the snow sample, that by definition is set to 273.15 K.

From Eq.(1), θ_w^M can be derived as follows (Kawashima et al., 1998)

$$\theta_w^M = \frac{M_s}{V_s \rho_w} \left(1 - \frac{C}{L} \left[\frac{(M_w + E)(T_w - T_f)}{M_s} - (T_f - T_s) \right] \right) \tag{2}$$

The freezing calorimeter operates on a similar principle to the melting calorimeter, however in this case the freezing agent and the container extract heat from the ice content and the LWC in the snow, causing it to freeze. The corresponding energy balance equation is given by:

$$\underbrace{Q_{freezing\ agent}}_{M_o^F C (T_f - T_o)} + \underbrace{Q_{Container}}_{M_c C_c (T_f - T_o)} + \underbrace{Q_{cooling\ ice}}_{M_i C_i (T_f - T_s)} + \underbrace{Q_{freezed\ LWC}}_{-M_{W_{LWC}} L} + \underbrace{Q_{cooling\ freezed\ LWC}}_{M_{W_{LWC}} C_i (T_f - T_s)} = 0 \tag{3}$$

Where, C_o is the heat capacity of the freezing agent, and C_i is the heat capacity of ice (2.09×10^3 J kg^{-1}K^{-1}). In the case of using silicone oil, C_o is 1.83×10^3 J kg^{-1}K^{-1} at $-10°C$.

https://doi.org/10.5194/egusphere-2023-2892
Preprint. Discussion started: 2 January 2024

In this case, the θ_w^F is directly related to the temperature difference induced by the freezing of water present in the snow and it is derived as shown in the following (Jones et al., 1983)

$$\theta_w^F = \frac{M_s}{V_s \rho_w} \left(\frac{(M_o + E) C_o (T_f - T_o)}{L M_s} - \frac{C_i (T_s - T_f)}{L} \right) \tag{4}$$

It is finally important to highlight that the determination of parameter E requires specific considerations. The introduction of E is necessary to account for the heat exchange that occurs between the snow sample and the internal walls of the calorimeter during the experiment. This imply accounting for conduction and radiation heat transfer mechanisms. In this study, we exclusively address heat conduction, assuming that the influence of radiation is negligible. In fact, the radiative transfer between the inner and outer wall is the most important energy loss factor of the calorimeter, but in the time-frame of the experiment i.e., few minutes this can be neglected. Therefore, as an inherent material property of the calorimeter, the computation of E can be accomplished as follows

$$E = \frac{M_{\text{cal}} C_{\text{cal}}}{C} \tag{5}$$

Where, M_{cal} and C_{cal} represent the mass and specific heat of the internal wall of the calorimeter, respectively. This method requires precise information about the calorimeter construction, which, in the case a commercial insulated container is used, can be obtained from the producer or by destructively analyzing the bottle itself. Alternative methods for estimating E are detailed in Appendix A. However, it is important to note that these methods, although non-destructive, are associated with significant uncertainties and are thus recommended to be avoided.

3 Propagation of the Uncertainty in Calorimetry

In scientific measurements, accounting for uncertainty propagation is crucial to accurately quantify the uncertainty associated with the obtained results (Moffat, 1988). The overall measurement uncertainty is influenced by a variety of factors, including instrumental uncertainties, environmental conditions and variations introduced by the operator during the experiment. Properly accounting and quantifying these sources of uncertainty is essential to ensure the reliability and validity of the LWC measurements using calorimetry.

In Section 3.1, we will initiate the uncertainty propagation analysis by focusing on the instruments uncertainty. The losses occurring during the experiment realization can be assumed to be equal both for melting and freezing calorimeter since the basic operations are analogous. This will enable a direct comparison between the melting and freezing calorimeters, reveling the suitability of the methods for real LWC measurements. In Section 3.2, we will extend the analysis to include uncertainties due to operator and environmental variations in the melting calorimetry. This is done by conducting repeated measurements done by different operators and under different conditions, which will also showcase both the method consistency and its accuracy. In Section 3.3, practical considerations pertaining to each step of the melting calorimetric experiment will be explored, focusing

https://doi.org/10.5194/egusphere-2023-2892
Preprint. Discussion started: 2 January 2024

on minimizing all sources of uncertainty. Finally, Section 3.4 shows the results of the sensitivity analysis of the melting calorimeter.

3.1 Instrumental uncertainty propagation: Melting vs Freezing Calorimetry

Instrumental uncertainty, which is arising from the limitations and imperfections of the measuring instrument itself, is propagating in the final estimation of LWC. In both melting and freezing calorimetry, the uncertainties are associated with temperature measurements and mass determinations. To quantify uncertainty propagation, statistical methods such as error propagation analysis are employed. In detail, the uncertainty $\sigma_{\theta_w^{M,F}}$ can be determined as the squared root of the sum of the squared partial derivatives of $\theta_w^{M,F}$ with respect to the variables with an associated uncertainty, each, multiplied by the squared associated error. The general formulation is reported in Eq. (6) (Moffat, 1988).

$$\sigma_{\theta_w^{M,F}} = \sqrt{\sum_{m_i} \left(\frac{\partial \theta_w^{M,F}}{\partial m_i} \right)^2 \sigma_{m_i}^2} \tag{6}$$

In Eq. (6), m_i represents a single measurement affected by uncertainty, and σ_{m_i} is the associated uncertainty. For the melting calorimeter, the required measurements are V_s, M_w, M_s, T_w, T_f and E (see Eq. (2)) with associated instrumental uncertainties σ_{M_w} and σ_{M_s}, which depends on the accuracy of the scale, σ_{T_w} and σ_{T_f}, which depends on the accuracy of the thermometer, σ_{V_s}, which depends on the uncertainties in measuring the volume of the sampler; and finally on σ_E, which depends on the uncertainty of the estimation of E (see Appendix A). Equation (6) can be applied to Eq. (2) and expanded as follows

$$\sigma_{\theta_w^M} = \sqrt{\left(\frac{\partial \theta_w^M}{\partial M_w} \right)^2 \sigma_{M_w}^2 + \left(\frac{\partial \theta_w^M}{\partial M_s} \right)^2 \sigma_{M_s}^2 + \left(\frac{\partial \theta_w^M}{\partial T_w} \right)^2 \sigma_{T_w}^2 + \left(\frac{\partial \theta_w^M}{\partial T_f} \right)^2 \sigma_{T_f}^2 + \left(\frac{\partial \theta_w^M}{\partial V_s} \right)^2 \sigma_{V_s}^2 + \left(\frac{\partial \theta_w^M}{\partial E} \right)^2 \sigma_E^2} \tag{7}$$

The partial derivatives in Eq. (7) are calculated as follows:

$$\frac{\partial \theta_w^M}{\partial M_w} = -\frac{M_s}{V_s \rho_w} \frac{C}{L} \frac{T_w - T_f}{M_s} \tag{8}$$

$$\frac{\partial \theta_w^M}{\partial T_w} = -\frac{M_s}{V_s \rho_w} \frac{C}{L} \frac{M_w + E}{M_s} \tag{9}$$

$$\frac{\partial \theta_w^M}{\partial T_f} = \frac{M_s}{V_s \rho_w} \frac{C}{L} \left(\frac{M_w + E}{M_s} + 1 \right) \tag{10}$$

$$\frac{\partial \theta_w^M}{\partial M_s} = \frac{M_s}{V_s \rho_w} \frac{C}{L} \frac{(M_w + E)(T_w - T_f)}{M_s^2} + \frac{1}{V_s \rho_w} \left(1 - \frac{C}{L} \left(\frac{(M_w + E)(T_w - T_f)}{M_s} - (T_f - T_s) \right) \right) \tag{11}$$

https://doi.org/10.5194/egusphere-2023-2892
Preprint. Discussion started: 2 January 2024

$$\frac{\partial \theta_w^M}{\partial V_s} = -\frac{M_s}{V_s^2 \rho_w}\left(1 - \frac{C}{L}\left(\frac{(M_w + E)(T_w - T_f)}{M_s} - (T_f - T_s)\right)\right) \tag{12}$$

$$\frac{\partial \theta_w^M}{\partial E} = -\frac{M_s}{V_s \rho_w}\frac{C}{L}\frac{T_w - T_f}{M_s} \tag{13}$$

Similarly, for the Freezing Calorimeter, we can analyze the error propagation associated with temperature and weight measurements of Eq. (4). In detail, by applying Eq. (6) we obtain

$$\sigma_{\theta_w^F} = \sqrt{\left(\frac{\partial \theta_w^F}{\partial M_o}\right)^2 \sigma_{M_o}^2 + \left(\frac{\partial \theta_w^F}{\partial M_s}\right)^2 \sigma_{M_s}^2 + \left(\frac{\partial \theta_w^F}{\partial T_o}\right)^2 \sigma_{T_o}^2 + \left(\frac{\partial \theta_w^F}{\partial T_f}\right)^2 \sigma_{T_f}^2 + \left(\frac{\partial \theta_w^M}{\partial V_s}\right)^2 \sigma_{V_s}^2 + \left(\frac{\partial \theta_w^F}{\partial E}\right)^2 \sigma_E^2} \tag{14}$$

The partial derivatives in Eq. (14) are calculated as follows:

$$\frac{\partial \theta_w^F}{\partial M_o} = \frac{M_s}{V_s \rho_w}\frac{C_o(T_f - T_o)}{L M_s} \tag{15}$$

$$\frac{\partial \theta_w^F}{\partial T_o} = -\frac{M_s}{V_s \rho_w}\frac{(M_o + E)C_o}{L M_s} \tag{16}$$

$$\frac{\partial \theta_w^F}{\partial T_f} = \frac{M_s}{V_s \rho_w L}\left(\frac{(M_o + E)C_o}{M_s} + C_i\right) \tag{17}$$

$$\frac{\partial \theta_w^F}{\partial M_s} = -\frac{1}{L}\left(\frac{(M_o + E)C_o(T_f - T_o)}{V_s \rho_w M_s} + \frac{1}{V_s \rho_w}\left(\frac{(M_o + E)C_o(T_f - T_o)}{M_s} - C_i(T_s - T_f)\right)\right) \tag{18}$$

$$\frac{\partial \theta_w^F}{\partial V_s} = -\frac{M_s}{V_s^2 \rho_w}\left(\frac{(M_o + E)C_o(T_f - T_o)}{L M_s} - \frac{C_i(T_s - T_f)}{L}\right) \tag{19}$$

$$\frac{\partial \theta_w^F}{\partial E} = \frac{M_s}{V_s \rho_w}\frac{C_o(T_f - T_o)}{L M_s} \tag{20}$$

By evaluating Eqs. (7) and (14) it is possible to compare the two methods as done in (Colbeck, 1978). In detail, by assuming $V_s = 200\ \mathrm{cm}^3$, a value consistent with the density measurement sampler (Proksch et al., 2016), which ensures compact dimensions for both the snow sampler and the calorimeter, facilitating transportation, and considering a snow density of the dry snow of $366\ \mathrm{kg\,m^{-3}}$, we set the temperature and mass of hot water at $40^\circ\mathrm{C}$ and 2 times M_s, respectively, in line with

https://doi.org/10.5194/egusphere-2023-2892
Preprint. Discussion started: 2 January 2024

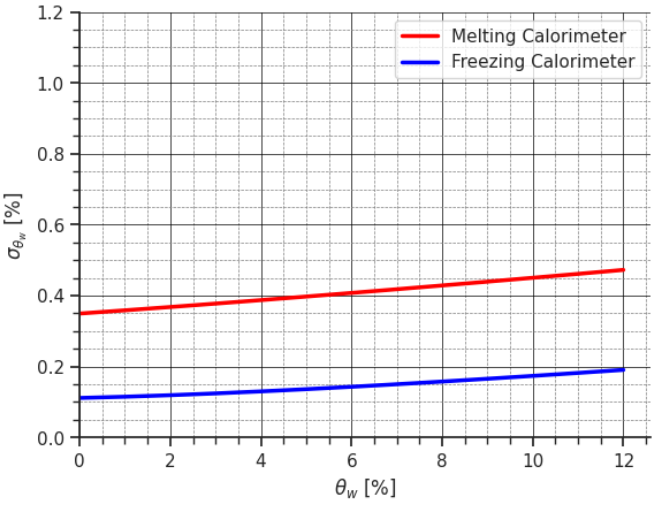

Figure 2. The figure provides a comparison of uncertainty in estimating LWC by propagating instrumental uncertainty using both the melting and freezing calorimeter methods. Notably, freezing calorimetry demonstrates lower uncertainty. However, it is essential to recognize that both methods offer uncertainties that still enable accurate measurement of LWC.

(Kawashima et al., 1998). Similarly, we set the temperature and mass of the freezing agent at $-30°\mathrm{C}$ and 1.3 times M_s, respectively, as per (Jones et al., 1983). The calorimetric constant was assumed to be equal to $6.58\mathrm{g}$. The LWC was varied from 0 to 12%, considering the most common values in melting snowpack. Additionally, we consider a scale with uncertainty of 0.1 g, a thermometer with uncertainty $0.2°\mathrm{C}$, an uncertainty in the estimation of the calorimeter constant E of 0.1 g. Regarding the uncertainty associated to the sample volume, to the best of our knowledge, no studies have been conducted in that specific direction. However from our practical experience a value of $2\ \mathrm{cm}^3$ can be realistic according to the tools we are using.

By substituting these values into Eqs. (7) and (2), we quantified the uncertainty associated to the LWC. The results are illustrated in Fig. 2. The comparison demonstrates the superior performance of the freezing calorimeter, particularly for high LWC values, where the melting calorimetry reach almost 0.5% uncertainty whereas the freezing calorimetry stops at 0.2% uncertainty. However, the general low value of $\sigma_{\theta_w^M}$, indicates that the melting calorimeter can still provide a significant and reliable measurement of LWC. Coupled with its notable practical advantages, the melting calorimeter becomes an attractive and compelling choice for field applications, particularly in remote areas.

It is finally important to highlight that, the uncertainty analysis presented here produces the same results as the paper of Colbeck (1978). By applying Eq. (7) for water saturation S_w, we can find that its relative uncertainty Σ_{S_w} is 5.1 times the relative uncertainty of the ice volume, whereas by applying Eq. (14), Σ_{S_w} is 0.84 times the relative uncertainty of the water volume, considering the values used in the original paper of Colbeck (1978). Nevertheless, it is essential to note that the relative uncertainty produced by the melting calorimeter on the estimation of the ice volume is one order of magnitude lower than the relative uncertainty produced by the freezing calorimeter on the water volume. This renders the final uncertainty of the two methods comparable, as shown in Fig. 2. All the details are reported in Appendix B.

https://doi.org/10.5194/egusphere-2023-2892
Preprint. Discussion started: 2 January 2024

3.2 Random uncertainty introduced by environmental factors and operator variations

After assessing the instrumental uncertainty of the melting calorimeter, it is crucial to consider the additional error sources that arise during the practical implementation of the experiment. These uncertainty sources primarily stem from the operator handling the various steps involved in the experiment, and the environmental factors at the measurement site. Quantifying these errors is challenging, but it is essential to establish a robust measurement protocol to minimize their impact. To quantify the impact of these sources of uncertainty we recruited a group of volunteers to perform a large number N of calorimetric experiment i.e., $N > 30$ following basic guidelines.

We designed the experiment utilizing an ice cube as a surrogate for snow samples. This approach provides a controlled means of assessing uncertainties stemming from sample preparation. Indeed, preparing the snow samples by introducing liquid water artificially into dry snow as done in (Kawashima et al., 1998) is a non-linear operation that requires the precisely estimation of the effects of this operation on the snow matrix introducing significant uncertainties on the effective LWC. On the contrary, using ice cubes allows to minimize the uncertainty in the sample preparation allowing to both i) appreciate the effectiveness of the melting calorimeter; and ii) proper characterize the effects of the operator variations in performing the calorimetric experiment under different environmental conditions.

The experimental setup, resembling the classic calorimetric experiment conducted in high school chemistry laboratories, aims to compare the measured final temperature ${T_f}^{\text{Exp}}$ of the mixture of hot water after the addition of the ice cube with the theoretical temperature T_f calculated using the calorimetric formula. Specifically, the experiment involved a predetermined mass M_i of ice at a known temperature T_i and a mass M_w of water at a known temperature T_w. The ratio between the ice mass M_i and the water mass M_w was kept constant to $\frac{1}{10}$.

As done in Eq. (1), in Eq. (21) we can express the experiment as an energy budget by equalizing the energy carried by the hot water ($Q_{hot\ water}$) and the internal wall of the calorimetry, in thermal equilibrium with the hot water ($Q_{Container}$), with the sinks consisting of the ice cube ($Q_{ice\ melting}$) and the melted ice ($Q_{melted\ ice}$).

$$\underbrace{Q_{hot\ water}}_{M_h^M C(T_f - T_w)} + \underbrace{Q_{Container}}_{M_c C_c (T_f - T_w)} + \underbrace{Q_{warming\ ice}}_{M_i C_i (T_f - T_i)} + \underbrace{Q_{ice\ melting}}_{LM_i} - \underbrace{Q_{melted\ ice}}_{M_i C (T_f - T_i)} = 0 \tag{21}$$

From the energy balance of Eq. (21) can be derived the final temperature T_f of the system as presented in Eq. (22).

$$T_f = \frac{C_i M_i T_i - L M_i + C(M_w + E) T_w}{C(M_w + E) + M_i C} \tag{22}$$

The associated experimental uncertainty $\sigma_{T_f}^{\text{Exp}}$, which is the sum of the instrumental uncertainty $\sigma_{T_f}^{\text{Ins}}$, the operator induced uncertainty $\sigma_{T_f}^{\text{Ope}}$ and the environment induced uncertainty $\sigma_{T_f}^{\text{Env}}$ that is

$$\sigma_{T_f}^{\text{Exp}} = \sigma_{T_f}^{\text{Ope}} + \sigma_{T_f}^{\text{Env}} + \sigma_{T_f}^{\text{Ins}} \tag{23}$$

https://doi.org/10.5194/egusphere-2023-2892
Preprint. Discussion started: 2 January 2024

In detail, the experimental uncertainty can be calculated as Root Mean Square (RMS) of the differences between the measured final temperature ${T_f}^{\text{Exp}}$ and the theoretical final temperature T_f as reported in Eq. (23).

$$\sigma_{T_f}^{\text{Exp}} = \sqrt{\frac{\sum_i^N (T_{f_i} - {T_{f_i}}^{\text{Exp}})^2}{N}} \tag{24}$$

Whereas, the instrumental uncertainty $\sigma_{T_f}^{\text{Ins}}$ is calculated using the approach introduced in Section 3.1, that for this specific case can be found as:

$$\sigma_{T_f}^{\text{Ins}} = \sqrt{\left(\frac{\partial T_f}{\partial M_i}\right)^2 \sigma_{M_i}^2 + \left(\frac{\partial T_f}{\partial T_i}\right)^2 \sigma_{T_i}^2 + \left(\frac{\partial T_f}{\partial M_w}\right)^2 \sigma_{M_w}^2 + \left(\frac{\partial T_f}{\partial T_w}\right)^2 \sigma_{T_w}^2} \tag{25}$$

Therefore the uncertainty associated to the operator variations $\sigma_{T_f}^{\text{Ope}}$ and the environmental factors $\sigma_{T_f}^{\text{Env}}$ can be retrieved by Eq. (23).

At this point, it is important to dig into a comprehensive analysis of these two distinct sources of uncertainty. Field campaigns often expose researchers or practitioners to challenging environmental conditions, encompassing factors such as wind, snowfall, or rain. The temperature spectrum can fluctuate significantly, spanning from sub-zero to positive values, thereby amplifying the potential for heat loss from the hot water and inducing changes in the sample phase, respectively. Additionally, the involvement of different operators, each potentially employing slightly varied techniques due to the different interpretations, introduces a layer of variability throughout the measurement procedure.

To take into account the influence of these uncertainty sources, we begin by examining the impact of wind on the measurement scale. Conducting an experiment involving subjecting the scale to a controlled breeze generated by a fan, we observe that the scale uncertainty escalates from 0.1 g to 1.5 g. This outcome translates to a corresponding $\sigma_{\theta_w^M}$ exceeding 1% across all conditions. Consequently, it is imperative to safeguard the scale against wind during experimentation; failure to do so renders the experiment result unreliable and the estimation of the uncertainty impossible. In case of scale shielded from wind σ_{M_w} and σ_{M_s} can be considered equal to the uncertainty of the scale.

To further simulate variations in air temperature and operator performance, we assemble a diverse group of individuals with varying expertise in the field of snow measurements. These participants are tasked with conducting measurements within an environment spanning temperatures from -5 to 20 °C. This multifaceted approach aims to capture the intricate interplay between operator influence and temperature differentials.

The outcome of the experiment is presented in Fig. 3. From a qualitative point of view, the figure demonstrates a good agreement between the measured and theoretical values indicating the effectiveness of the melting calorimetry. The small spread of the data indicate that the experimental is largely reproducible among different operators. The missing of a bias indicate that there are no large systematic errors. From a quantitative point of view the RMSE, $\sigma_{T_f}^{\text{Exp}} = 0.5°\text{C}$ on the final temperature T_f, compared to the $0.2°\text{C}$ instrumental error, $\sigma_{T_f}^{\text{Ins}}$ alone. Resulting in $\sigma_{T_f}^{\text{Ope}} + \sigma_{T_f}^{\text{Env}} = 0.3°\text{C}$. Importantly, when neglecting the term E in Eq. (25) the omission leads to a bias of $-0.2°\text{C}$. This overestimation distinctly showcases the systematic uncertainty induced by failing to account for the heat transferred to the internal calorimeter walls.

https://doi.org/10.5194/egusphere-2023-2892
Preprint. Discussion started: 2 January 2024

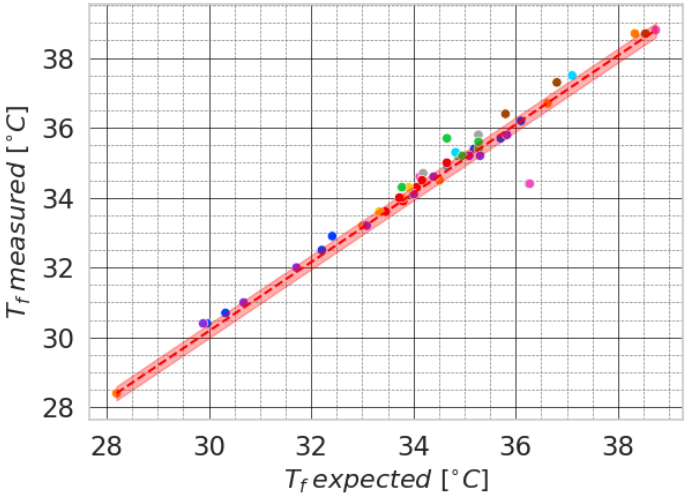

Figure 3. Results of the calorimetric experiment performed by a group of volunteers. The measured final temperature (y-axis) is compared with the theoretical final temperature (x-axis) derived from Eq. (22). The different colors of the dots represent the different people who performed the experiment. The red area represent the instrumental uncertainty of all the measurements using Eq. (25).

Given the fact that the steps of this experiment are exactly the same of the steps for the derivation of LWC using Eq. (2), we can use the derived $\sigma_{T_f}^{\text{Ope+Env}}$ to update the uncertainty calculated in Section 3.1 by adding this uncertainty to the final temperature measurement σ_{T_f}. In Fig. 4, we observe how this new characterization of the uncertainty affects the uncertainty in the estimation of LWC with respect to only considering the instrumental showing a more realistic value that is ranging from about 0.8% to 1% for the parameters listed in Sec. 3.1. A similar analysis could be applied to the freezing calorimeter, considering the losses associated with the measurement time required by this technique. However, this is beyond the scope of the paper.

3.3 Minimizing the Instrumental Uncertainty of the Melting Calorimetry

Now that the main source of uncertainty have been analyzed, it is possible to make some important considerations on how to decrease the overall uncertainty of the melting calorimetry. As described in Section 2, some of the variables involved in the calorimetry are free to be selected during the experiment. These are V_s, M_s, M_w, T_w, and E. However, all these variables are strictly connected to each other with some implications that it is better to account for.

Firstly, by increasing the volume sample V_s, one is expecting that the uncertainty is decreasing being V_s at the denominator for all the terms in Eq. (7). Nonetheless, the volume of the sample is linked to its mass, which increases by increasing the volume. This has an effect of compensation on σ_w^M, which stabilizes around 0.46% for samples exceeding $100\,\text{cm}^3$. This outcome paves the way for dedicated investigations into employing various sample volumes for characterizing liquid water transport within the snowpack. Although such research lies outside the scope of this paper, we provide here some ideas that

https://doi.org/10.5194/egusphere-2023-2892
Preprint. Discussion started: 2 January 2024

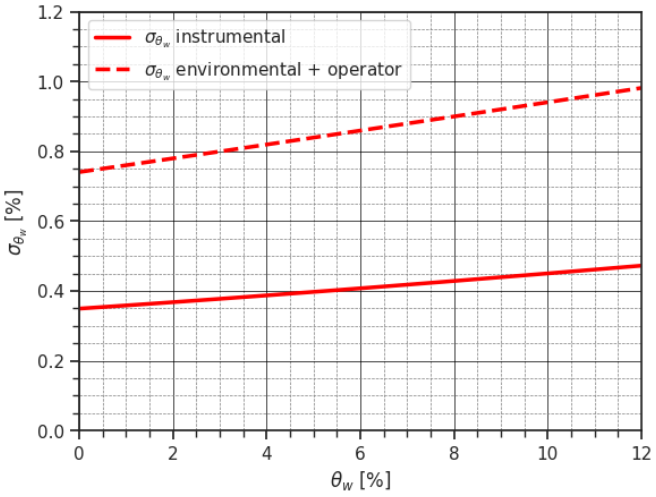

Figure 4. Comparison of the propagation of uncertainty considering the instrumental uncertainty (solid red line) and random uncertainty introduced by variations in operators and environmental factors (dashed red line) for the melting calorimeter.

explain the volume selected in the context of this paper. As discussed in Section 3.1, V_s is generally constrained by the snow sampler used, which is normally fixed e.g., the Taylor–LaChapelle density cutter. Similarly with the measuring of the density (Proksch et al., 2016), V_s is selected focusing primarily on the resolution required to describe LWC in the snowpack: a small snow cutter allows to sample the small difference in LWC within the snowpack, whereas a large volume density sample provides snowpack bulk information. Given the high heterogeneity of LWC (Techel and Pielmeier, 2011), one can think of sampling the snowpack with a high vertical and horizontal resolution. This however requires performing a large number of calorimetric analysis, which may require a time for which it is not possible to assume that LWC did not change (for example, to avoid this, by employing a parallel team of students in 1967, Yosida perform 120 measurements to describe the temporal evolution of a 160 cm snowpack over 7 hours highlighting that an average of 20 mins are required for each measurements). On the contrary, taking a snow sample that is big poses some challenges for both the selection of the calorimeter, which generally features a small aperture (see Fig. 1) and the possibility to represent specific cases such as the situations of water saturation on top of ice layers. In practice, by considering a calorimeter with capacity of $0.5\mathrm{L}$, V_s should fall between 100 and 300 cm^3. For melting snow, this corresponds to a M_s that ranges approximately between 60 and $150\mathrm{g}$. Within these values the influence of V_s on the overall uncertainty σ_w^M is limited. For samples of this volume, it is advisable to prioritize a smaller vertical footprint—such as a cylindrical sampler with a diameter of $4\ \mathrm{cm}$ and a depth of $18\ \mathrm{cm}$—over a shallower penetration depth with a larger vertical footprint. This strategy aids in identifying saturated layers and ensures smoother insertion of the snow sample into the calorimeter i.e., diameter of the sampler $<$ opening of the calorimeter.

https://doi.org/10.5194/egusphere-2023-2892
Preprint. Discussion started: 2 January 2024

At this point, the remaining variables are M_w, T_w, and E. It is then mathematically convenient to introduce a new variable as done in (Kawashima et al., 1998) i.e.,

$$R = \frac{M_w}{M_s} \tag{26}$$

This allows us to plot the uncertainty in function of the temperature of water and the ratio between the masses for different level of LWC and using different calorimeter constants (see Fig. 5). Considering a $V_s = 200cm^3$, a dry snow density of $366\mathrm{kgm}^{-3}$ and a calorimeter with $E = 6.58$ g it is possible to show that low value of R i.e. a same mass of hot water and snow and high water temperature T_w are then one that produce the best results in terms of uncertainty. However, high T_w means a large temperature loss when the calorimeter is open to insert the snow sample. To minimize this loss, that otherwise has to be considered in the calorimetric formulation, a T_w of 40 to 50 degree Celsius together with a quick insertion of the snow sample in the calorimeter, is a good trade-off for all the possible cases as indicated by (Kawashima et al., 1998). On the other hand it is worth stressing the fact that, even though low values of R produce the best results, this has two practical implications that should not be neglected: i) if an immersion thermometer is used (as the one represented in Fig. 1) a particular attention should be devoted to the fact that the probe is properly immersed inside the water-snow mixture. Otherwise the temperature measure will oscillate. Therefore, especially if the calorimeter is very tall and the snow sampler is small and cannot be increased, M_w should be increased. This may allow a proper immersion of the temperature probe inside the snow-water mixture. ii) If the snow sample is too big with respect to the water mass, or the water temperature is too low, the heat exchange cannot be completed i.e., $T_f < 0°\mathrm{C}$. As recommendation we advise to keep $T_f > 5°\mathrm{C}$. A value of $R = 2$ is a good trade-off for all the possible real cases (see Fig. 5).

Finally it is important to mention that different value of E imply a change in the uncertainty. However, as we stress the fact that this change is limited and therefore different size, shape and quality of calorimeter can potentially be employed. Differently, a wrong estimation of the calorimeter constant can have a big impact on the accuracy of the measure of LWC.

3.4 Sensitivity Analysis of the Melting Calorimetry

By studying Eqs. (8)-(13) we can derive important information about the sensitivity of melting calorimetry to variation of the input variables V_s, M_s, M_w, T_w, and E. In fig.6 is reported the variation in the LWC θ_w^M associated to the change of the experiment parameters for a realistic case where the snow density is $416\mathrm{kgm}^{-3}$, $M_s = 83.4$g, $M_w = 166.8$g, $T_f = 4.8°\mathrm{C}$, $T_w = 40°\mathrm{C}$, $E = 6.58$g and $\theta_w^M = 5.0\%$.

Figure 6a illustrates that the error in volume measurement is directly proportional to LWC. However, the impact of this error is relatively limited. For instance, in the considered scenario where a snow cutter with dimensions of $4 \times 2.75 \times 18\mathrm{cm}^3 = 198\mathrm{cm}^3$ is employed and a portion of $20\mathrm{cm}^3$ is lost due to incomplete filling i.e., the snow cutter is not filled to a depth of $2\mathrm{cm}$, the resulting LWC measurement is overestimated by a mere 0.10%. This suggests the feasibility of utilizing snow samplers with variable depth, such as samplers with moving piston, to adapt the sample size according to LWC distribution in the snowpack.

In Fig. 6b, one can observe how even a small error of a few grams in the measurement of hot water mass can significantly impact the resulting LWC, causing a nearly 1 percentage point difference. This highlights the crucial significance of ensuring

https://doi.org/10.5194/egusphere-2023-2892
Preprint. Discussion started: 2 January 2024

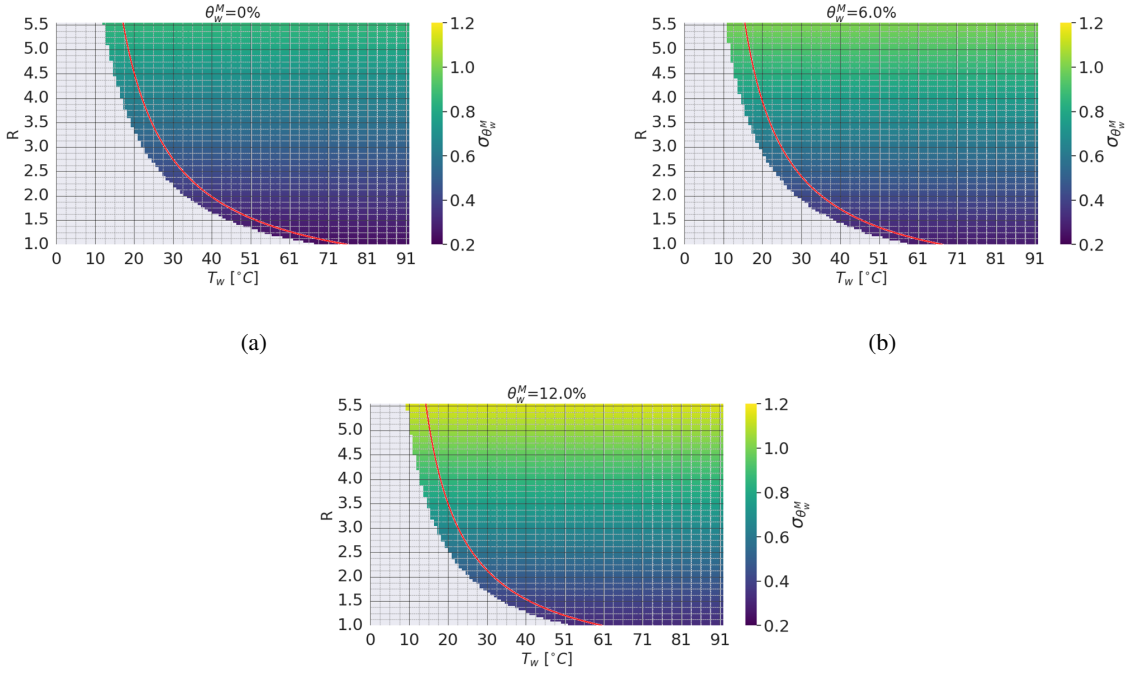

Figure 5. In the figure is presented the uncertainty associated to θ_w^M as a function of the experiment parameter R and T_w. In detail the uncertainty is presented for 3 representative scenarios of θ_w^M i.e., 0%, 6%, and 12%. In (a) is presented the dry snow scenario with $\theta_w^M = 0\%$; in (b) is presented the medium wetness scenario with $\theta_w^M = 6\%$ and in (c) is presented the limit wetness scenario with $\theta_w^M = 12\%$. Gray area represent the cases where the calorimetric experiment results in a final temperature lower than $0°\mathrm{C}$. The indicated red boundary signifies a "safety" threshold constrained by a final temperature of $5°\mathrm{C}$, i.e. the points laying on the red line result in a $T_f = 5°\mathrm{C}$. When working on the left side of the curve, we are pushing the limits of experimental feasibility. Therefore, it is advisable to exercise caution and strive to remain on the right side of this boundary. In all cases, high values of R are associated with high uncertainty.

a stable and well-prepared position for the scale, protected by the influence of wind gusts by a well dug snow pit and an additional shield. In the end the plate of the balance should be sufficiently large compared to the calorimeter.

The accurate measurement the hot water temperature is equally important (see Fig. 6c). An overestimation of $1°\mathrm{C}$ in T_w results in an approximate 1% underestimation of θ_w^M. Additionally, it is crucial to emphasize the importance of measuring T_w only after the entire calorimeter has reached temperature stability. Using a well-insulated container and promptly inserting the snow sample into the calorimeter, so that the hot water is not losing temperature, are vital factors to minimize errors in the measurement of T_w. The specification regarding the depth of immersion for the thermometer probe must be satisfied.

The misreading of T_f leads to a directly proportional error in the final LWC measurement (see Fig. 6d). Achieving an accurate measurement of T_f necessitates ensuring that the heat exchange process is fully completed. To facilitate this, gently

https://doi.org/10.5194/egusphere-2023-2892
Preprint. Discussion started: 2 January 2024

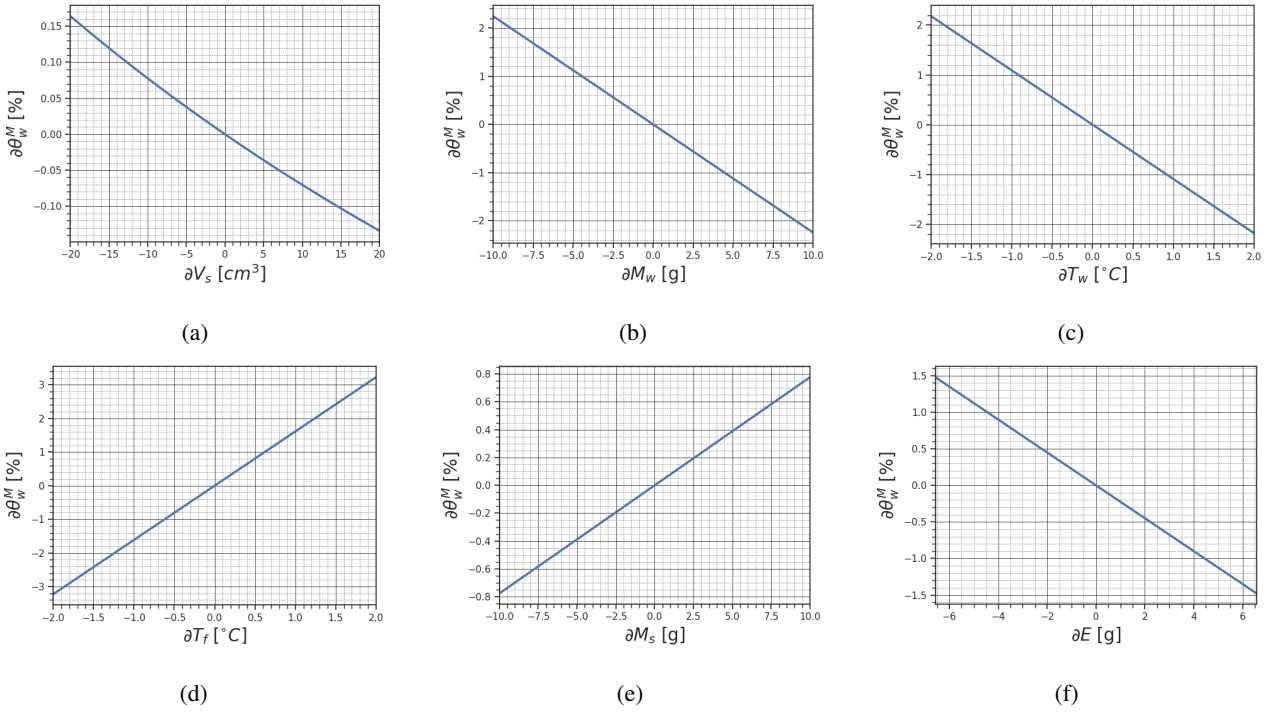

Figure 6. In the figure is reported the variation of θ_w^M with respect to the six parameters that define the experiment. In detail in (a) is reported the variation of θ_w^M with respect to V_s, in (b) is reported the variation of θ_w^M with respect to M_w, in (c) is reported the variation of θ_w^M with respect to T_w, in (d) is reported the variation of θ_w^M with respect to T_f, in (e) is reported the variation of θ_w^M with respect to M_s and in (e) is reported the variation of θ_w^M with respect to E.

shaking the calorimeter is recommended, and the completion of the process can be verified by observing a clear stabilization in the temperature reading. This is usually occurring within 30 seconds after inserting the snow sample into the calorimeter.

An error in the mass measurement of the snow sample M_s introduces a directly proportional error in θ_w^M (see Fig. 6e). To ensure accurate measurements, the same precautions as those taken for the measurements of M_w should be followed.

340 Finally, it is crucial to note that an error in E is inversely proportional to the LWC (see Fig. 6f). Neglecting the heat exchange with the calorimeter wall, i.e., assuming $E = 0$g, results in significant errors in the final measurement of θ_w^M. Therefore, when using a new calorimeter, proper time and effort should be dedicated to accurately estimating E, as described in Section 3.1.

The selection of the values will be summarized in section 4 in form of a protocol that all the research and practitioners can follow during field experiments.

https://doi.org/10.5194/egusphere-2023-2892
Preprint. Discussion started: 2 January 2024

4 Melting Calorimeter Protocol

In this section, we will provide a comprehensive summary of the analyses conducted throughout the paper and propose a practical measurement protocol to be followed during field campaigns. First, the necessary materials need to be prepared, including:

Calorimeter This could be a commercially available insulated container designed to maintain the temperature of beverages or food. The calorimeter constant must be known or derived for accurate measurements (e.g., with Eq. (5)). In this work we used a commercial insulated container i.e., Stanley Classic Legendary Food Jar made of stainless steel (i.e., SAE 304) $C_{\text{cal}} = 500\ \text{Jkg}^{-1}\,\text{K}^{-1}$ and $M_{\text{cal}} = 69.1$ g, $E = 6.58$ g. The uncertainty of this measurement is only related to the uncertainty of the scale used to weight the container i.e., 0.1g.

High-Precision Immersion Thermometer Used to monitor temperature changes during the experiment.

Precision Balance Utilized for measuring the mass of hot water and snow samples. The scale should be at least splash proof (IPX4).

Supportive Surface A hard, supportive surface such as Plexiglass.

Wind Shield A well dug shelter or an external barrier, such as a plexiglas container can be used to shield the scale from wind.

Insulated bottle The bottle acts as a reservoir of hot water, ensuring a continuous supply for the experiment

Snow sampler This can be any of the available snow sampler for density measurements. The shape and size of the sampler must match the shape and size of the calorimeter.

The snow pit should be dug so that the snow wall is shaded from the sun. Once the snow pit is prepared, a shaded area for the scale should be established (see Fig. 7a), protecting it from solar radiation and wind. Another hole should be dug for storing the snow sampler and auxiliary tools needed for sample preparation in order to maintain them at low temperatures. The outer surface of the pit profile should be smoothed, and the bottom should be level to ensure accurate measurement of the snow height at which the LWC measurement will be taken.

Following these preparations, the following steps should be followed:

1. Warm up the water at the temperature of 40 to $50°\text{C}$ and store it in the insulated bottle;
2. Tare the scale with the calorimeter and the lid with the thermometer on top;
3. Prepare the hot water inside the calorimeter in a quantity that meets the minimum immersion requirement of the thermometer and is approximately two times the sample mass (annotate it as M_w); If a volume of 200cm^3 is used, approximately 200g of hot water should be used;
4. Close the calorimeter and wait for the temperature to stabilize;

https://doi.org/10.5194/egusphere-2023-2892
Preprint. Discussion started: 2 January 2024

(a)

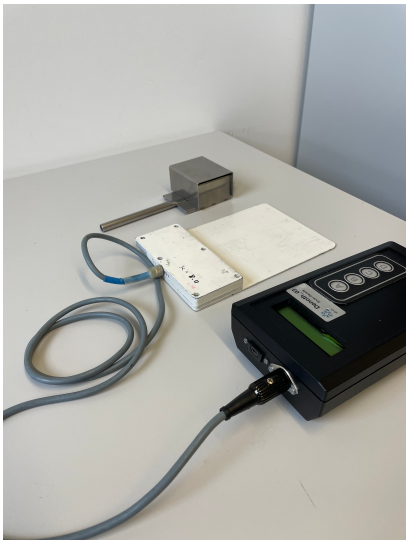

(b)

Figure 7. In (a) is reported the essential materials for the melting calorimeter experiment. From left to right: the insulated container where heat exchange occurs, its thermometer, the thermos storing the hot water used in the experiment, and the scale for measuring mass placed on a stable plexiglass panel. In (b) is reported from left to right, the snow cutter, used for sampling the snowpack at the Weissfluhjoch site and the Denomether used during the measurement campaign.

5. Record the temperature T_w. It should be around $40°\mathrm{C}$;
6. Tare the scale with the calorimeter and hot water (otherwise the uncertainty of the two measurements must be propagated through eq.(6)).
7. Retrieve the snow sampler from the shaded hole and collect a snow sample from the designated height, ensuring no phase changes occur (i.e. take the sample on shade) or any loss;
8. Open the calorimeter and place the snow sample inside. Minimize the time for this step;
9. Gently shake the calorimeter;
10. Weigh the snow mass M_s by placing the calorimeter on the tared scale waiting for the temperature to stabilize;
11. Once the temperature stabilizes, approximately 1 minute after sample insertion, read the temperature T_f.
12. Empty and dry the calorimeter for subsequent measurements.

By following this protocol meticulously, the measurement of LWC in the snowpack can be conducted with the accuracy and the uncertainty showed in this paper.

https://doi.org/10.5194/egusphere-2023-2892
Preprint. Discussion started: 2 January 2024

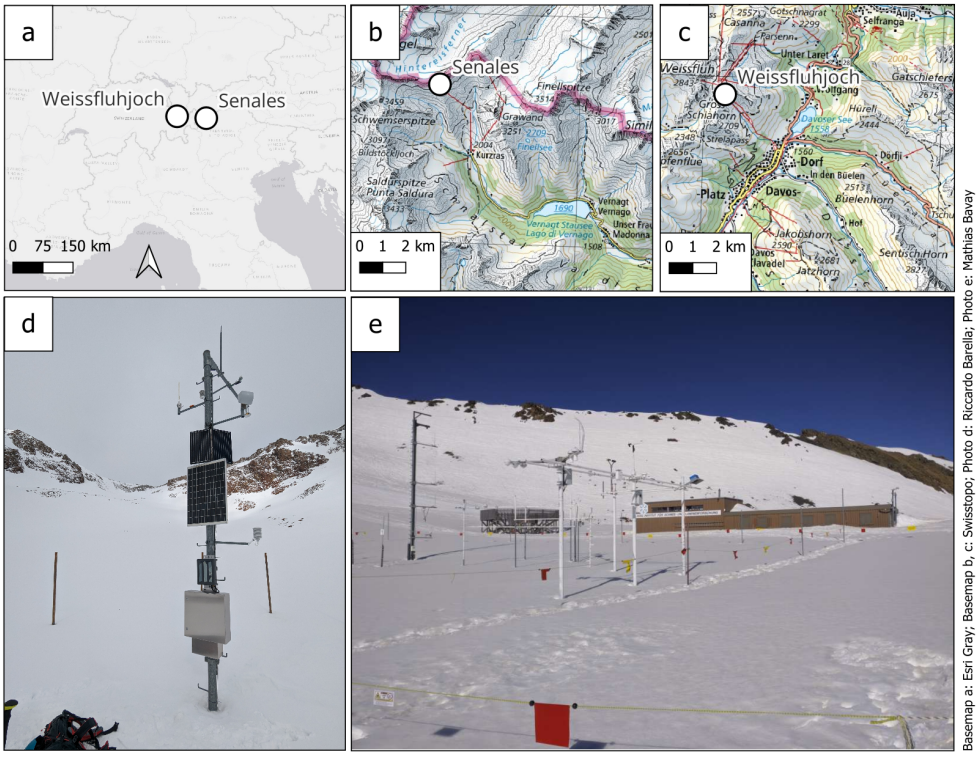

Figure 8. The figure gives an overview of the two sites used for tsting the calorimeter. Ia a) the two sites can be visualized in the Alpine context, while in b) and c) the Weissfluhjoch and Senales sites can be respectively visualized in the local context. In the end in d) is shown a picture of the senales site and in e) is shown a picture of Weissfluhjoch site.

5 Experimental Application of the Melting Calorimeter protocol: LWC Profiles in the Field

To assess the performance of the calorimeter in field conditions and refine the measurement protocol, a series of field activities were conducted. These activities aimed to test the accuracy and reliability of the calorimeter protocol in real snowpack and with real conditions. The field tests were carried out in Val Senales (Italy) (see Fig. 8b-d) and at the Weissfluhjoch (Swiss) (see Fig. 8c-e) with different melting snow packs, including different snow densities and liquid water content levels spanning the period from April to June 2023. In order to asses the validity of the calorimetric measurements of LWC, additional measurements of density, specific surface area (SSA), stratigrafy, infrared imaging (IR), and LWC conducted with the Denothmeter (Denoth and Foglar (1986)) were acquired. The large number of measurements allowed to fine-tune the operations in the field according to the protocol and minimizing the disturbance caused during sample collection allowing to compare the different measurements.

https://doi.org/10.5194/egusphere-2023-2892
Preprint. Discussion started: 2 January 2024

5.1 Weissfluhjoch

The field tests performed in Switzerland were carried out at the field site of Weissfluhjoch (2536 m a.s.l.) in the area of Davos (Graubünden). In addition to being a high-altitude research station for which there is one of the longest observed time series in the world (Marty and Meister, 2012). It lies on a wide flat area partially sheltered from wind, the research field is fenced to safeguard the snow surface as much as possible from outside intrusion and disturbance, and finally, two huts are made available to the operator, providing shelter and tools, as well as electricity, heating and internet connection. These features make the research field particularly suitable for performing high-level measurement campaigns for various types of snowpacks.

LWC measurements carried out at the Weissfluhjoch field site are part of a comprehensive measurement campaign which took place over the course of the winter season 2022-2023. The measurement campaign started on 14 February and lasted until 16 June 2023. At the beginning of the campaign, the recorded snow height was $108\ \mathrm{cm}$; on the last day of measurements, it was $50\ \mathrm{cm}$. The maximum recorded snow height during a campaign day was $192\ \mathrm{cm}$. Measurements have been performed every second day, for a total of 36 days of measurements. A wide set of variables was measured (Snow Water Equivalent; profiles of snow temperature, density, permittivity, Specific Surface Area; snow roughness) using manual, electromagnetic and remote sensing systems. The vertical resolution of the snow temperature, density, permittivity and Specific Surface Area profiles is very high: measurements were taken each 10, 4, 3 and $2\ \mathrm{cm}$, respectively.

Figure 9 describes the state of the snowpack at the field site of Weissfluhjoch through some properties sampled with vertical profiles on the day of 22 May 2023. The measurements started at 08:00 Local Time (LT) in the morning underneath an overcast sky. The measured air temperature was $7\ ^{\circ}\mathrm{C}$ and a neglegible wind was blowing from North at a speed of $1\ \mathrm{km\,h^{-1}}$. The height of the snowpack was $164\ \mathrm{cm}$, the surface was smooth, and no new snow had fallen in the previous 24 hours. The temperature profile sampled every $10\ \mathrm{cm}$ from top to bottom showed that the snowpack was fully isothermal. The Near Infra-Red (NIR) photograph reported in Figure 9e illustrates quite a complex snowpack stratigraphy on that day, which along with the stratigraphic observations helps to get a qualitative idea about general conditions and local peculiarities. It is important to notice that even though the NIR image was aligned with the LWC and density profiles through a rigorous co-registration procedure, ensuring that the meterstick depicted in the middle of the images aligns with the y-axis of the plots, the stratigraphic features of the snowpack and the vertical profiles shown in Fig. 9 were sampled one next to each other along an approximately 2-meters wide wall. Given the irregularity of the layers, the location of the ice lenses recorded in the field and shown in Fig. 9 does not match perfectly with the NIR image.

Figure 9e is annotated with qualitative comments about the state of the snowpack on the measurement day, in terms of wetness, layers and types of grains. Surface melt was observed on the superficial layer, blocked by a layer of transformed snow. Between H=124 cm and H=121 cm, the first ice lens was observed. Between the first ice lens and the upper transformed layer, the snow seemed drier than on the surface. Other dry layers were observed until H=98 cm, spaced out by two more ice lenses. Just below the last ice lens the snow seemed dry, but it was observed to become wetter towards the ground. Finally, water runoff was found on the bottom of the snow pit. Figure 9(a) and 9(b) show the LWC sampled with the melting calorimeter and with the Denoth every 5 and 2 cm, respectively; Fig. 9(c) shows the snowpack density sampled every 3 cm with the snowcutter; Fig. 9(d)

https://doi.org/10.5194/egusphere-2023-2892
Preprint. Discussion started: 2 January 2024

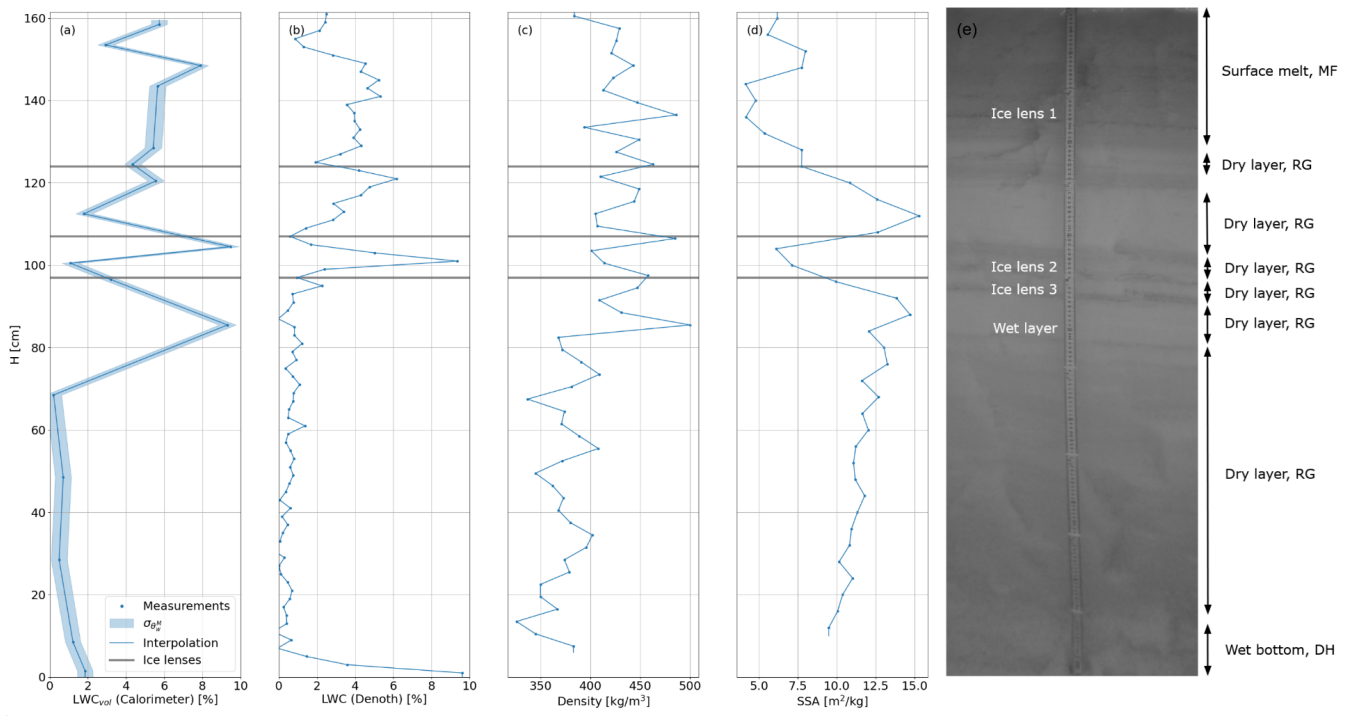

Figure 9. Snow profile at Weissfluhjoch on 22 May 2023. Panel (a) shows the volumetric LWC profile sampled every 5 cm with the melting calorimeter and its associated uncertainty computed with Eqs. (2) and (7). Panel (b) shows the LWC profile sampled every 2 cm with the Denothmeter. Panel (c) shows the snow density sampled every 3 cm with the snowcutter. Panel (d) shows the Specific Surface Area profile sampled every 4 cm with the SLF InfraSnow sensor. Panel (e) is the co-registered Near Infra-Red picture on a greyscale taken on the same day before starting the measurements: different reflectance values in the picture identify differences in optical equivalent grain size. Layers are indicated according to the wetness, whereas acronyms refer to the official classification of snow on the ground (Ice, 1990): MF refer to melt forms, RG to rounded grains, DH to depth hoar. On the panels, bullet points represent measurements, lines connecting them are linear interpolations, grey lines represent the position of the ice lenses as visually detected in the field.

shows the Specific Surface Area (SSA) sampled every 4 cm by means of the SLF InfraSnow sensor (FPGA Company). Surface melt is captured by both the calorimeter and the Denoth, although the LWC on the surface measured with the calorimeter is notably higher. The layer of transformed snow is highlighted by LWC values between 4 and 5% (i.e. the maximum water retention capacity of snow) by both the calorimeter and the Denoth, which basically agree considering the possible natural variations. Ice lenses are characterized by drops in LWC values (this is particularly well observed with the Denoth because of its higher measurement vertical resolution) and a locally higher density. Ice lenses are observed to block the drainage of the LWC to the bottom: in between ice lenses the snow is drier and characterized by a drop in LWC which can be observed with both the calorimeter and the Denoth (Fig. 9(a) and 9(b)), a local decrease in density (Fig. 9(c)) and a local increase in SSA, which increases with smaller and drier grains (Fig. 9(d)).

https://doi.org/10.5194/egusphere-2023-2892
Preprint. Discussion started: 2 January 2024

Figure 9(a) shows a very high LWC value at 87 cm from the bottom. As can be qualitatively observed from the NIR picture in Fig. 9(e), that height coincided with an extremely wet layer of snow. This was well captured by the calorimeter and can be confirmed by the fact that at that height the highest snow density and SSA were recorded (Fig. 9(c) and 9(d), respectively). Interestingly, despite the high vertical resolution of the measurements, the Denoth seemingly did not identify this wet layer. This can be also due to a very localized point of water saturation. Finally, the LWC values measured by both the calorimeter and the Denoth show that from H=87 cm to the bottom, the snowpack is releasing meltwater: from close to zero, values increase to 2 and 10% at the bottom, respectively. The release of water can be also observed as a gradual decrease of snow density below the highest value measured at H=87 cm and, qualitatively, in a gradual decrease of SSA.

5.2 Schnalstal

The Italian test site is located in Schnalstal, in South Tyrol. This site has been chosen because the high altitude (∼3000m) guarantees the presence of abundant snow and a long-lasting melting season, and it is well-served by lifts and roads, making it easy to access.

The snowpack at the Schnalstal field site, with a height of 79 cm, was profiled on 7 June 2023, at 12:30 LT. During the measurements, the air temperature stood at 1.8 cm, and there was negligible wind speed, ensuring relatively stable conditions for the assessment. The snowpack structure was as follows: from the surface down to 65 cm, a layer of recent snow was observed, which had undergone wetting due to temperature and solar radiation, which were relative high that day. The subsequent layer, spanning from 65 cm to 57 cm, contained three prominent ice lenses. Notably, a significant amount of LWC was trapped within this layer, contributing to its distinctive characteristics.

Continuing downwards, the layer from 57 cm to the base at 0 cm was characterized by coarse snow crystals with size from 1 to 2 mm, exhibiting lower water retention capability. Importantly, there was no noticeable LWC presence within this layer. However, the lowermost 20 cm of the snowpack presented some noticeable challenges. This section displayed loose and coarse crystals, leading to difficulties in proper sampling and ensuring optimal coupling between the Denoth instrument and the snow. Consequently, these lower 20 cm were excluded from the subsequent analysis to ensure data accuracy and reliability.

Figure 10 (a) depicts the volumetric liquid water content (LWC) profile, measured with the melting calorimeter technique, along with its corresponding uncertainty, as computed using Eqs. (2) and (7). Panel (b) of the figure portrays the LWC profile derived from Denoth measurements. Panel (c) showcases the snow density associated with the measurement points obtained from the calorimeter. These profiles collectively provide valuable insights into the internal structure of the snowpack and its distribution of liquid water. Specifically, the LWC profile reflects the typical conditions in 2023 of the European alpine snowpacks, where ice lenses were often present. Despite a significant amount of snowfall occurring in spring, the melting process was hindered by the presence of these ice lenses, impeding the transport of water to the ground. Finally we can notice how the Denothmeter is underestimating the superficial LWC as for WFJ.

https://doi.org/10.5194/egusphere-2023-2892
Preprint. Discussion started: 2 January 2024

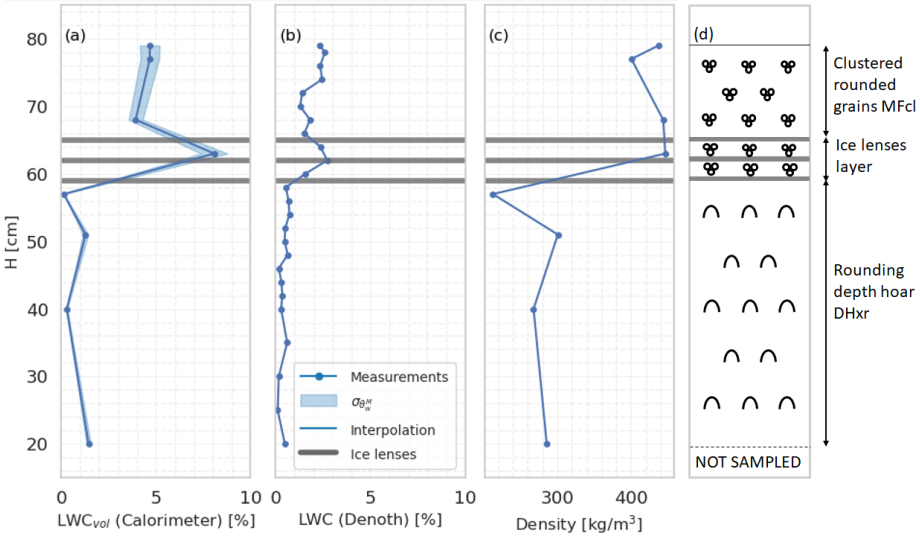

Figure 10. Snow profile at Schnalstal on 7 June 2023. Panel (a) displays the volumetric LWC profile generated using the melting calorimeter, including its associated uncertainty calculated through Eq. (2). Panel (b) exhibits the LWC profile sampled with the Denoth. Panel (c) illustrates the snow density associated with the calorimeter measurement points. In panel (d) in the end it is reported a scheme of the profile since for that site no IR photos were available.

6 Conclusions

The potential of melting calorimetry for measuring snow LWC has long been overshadowed by misconceptions about its accuracy.

This paper, challenged this perception by comparing the melting and freezing calorimetry techniques, focusing on their applicability for measurements in the field. Our findings indicated that the measurements obtained using the melting calorimeter are still accurate enough for an meaningful analysis of LWC in the snowpack, offering at the same time notable practical advantages. To support our claims, we had thoroughly examined and propagated uncertainties, encompassing not only instrumental factors but also variations arising from the operational procedures and environmental conditions. As a result, we devised a field protocol that effectively minimizes these uncertainties. The protocol includes specific instructions on the amount of hot water to be used, its temperature, the size of the calorimeter, the masses involved, and other crucial details for controlling the uncertainty during the experiment replication. This protocol was applied in two different test sites in Italy and Switzerland by two different research groups with different melting calorimeters. The results, compared to independent measurements of dielectric constant of the snow, showed how the application of the proposed protocol to the melting calorimeteric measurements is able to properly track the wet front penetration inside the snowpack in an accurate way.

In conclusion, this research encourages the wider adoption of melting calorimetry as a valuable tool for quantifying liquid water content in snowpacks.

https://doi.org/10.5194/egusphere-2023-2892
Preprint. Discussion started: 2 January 2024

Code and data availability. The code to calculate LWC and its uncertainty from the melting calorimetry analysis will be made available along with the code for generating the figures in the paper in a dedicated GitLab of the Snowtinel project.

Appendix A

In order to derive the calorimetric constant E, if information regarding the material and mass of the calorimeter cannot be obtained, the heat-balance principle can be applied. In the literature, the calorimeter constant is typically determined using a basic heat-balance principle (Jones et al. (1983); Austin (1990)). When warm fluid is mixed with cold fluid in the calorimeter bottle, the heat lost by the warm fluid must be equal to the heat gained by the cold fluid and the bottle itself.

For the case of water, the heat-balance equation is given by:

$$\underbrace{Q_{hot\ water}}_{M_h C(T_f - T_w)} + \underbrace{Q_{cold\ water}}_{M_c C(T_f - T_c)} + \underbrace{Q_{Container}}_{M_c C_c (T_f - T_c)} = 0 \tag{A1}$$

Therefore we can obtain the calorimetric constant expresed in equivalent water mass as follows

$$E = \frac{M_h(T_f - T_h)}{(T_c - T_f)} - M_c \tag{A2}$$

In this equation, M_h and T_h represent the mass and temperature of the hot water, while M_c and T_c represent the mass and temperature of the cold water, respectively. By analyzing the uncertainty propagation of the measurements on E with the same approach presented in 3.1 we can retrieve the uncertainty on the estimation of E, σ_E:

$$\sigma_E = \sqrt{\left(\frac{\partial E}{\partial M_h}\right)^2 \sigma_{M_h}^2 + \left(\frac{\partial E}{\partial M_c}\right)^2 \sigma_{M_c}^2 + \left(\frac{\partial E}{\partial T_h}\right)^2 \sigma_{T_h}^2 + \left(\frac{\partial E}{\partial T_f}\right)^2 \sigma_{T_f}^2 + \left(\frac{\partial E}{\partial T_c}\right)^2 \sigma_{T_c}^2} \tag{A3}$$

The partial derivatives in Eq. (A3) are calculated as follows:

$$\frac{\partial E}{\partial M_h} = \frac{T_f - T_h}{T_c - T_f} \tag{A4}$$

$$\frac{\partial E}{\partial M_c} = -1 \tag{A5}$$

$$\frac{\partial E}{\partial T_h} = -\frac{M_h}{T_c - T_f} \tag{A6}$$

https://doi.org/10.5194/egusphere-2023-2892
Preprint. Discussion started: 2 January 2024

$$\frac{\partial E}{\partial T_f} = \frac{M_h(T_c - T_f) + M_h(T_f - T_h)}{(T_c - T_f)^2} \tag{A7}$$

$$\frac{\partial E}{\partial T_c} = -M_h \frac{T_f - T_h}{(T_c - T_f)^2} \tag{A8}$$

It becomes evident that σ_E is strongly related to the difference $T_f - T_c$, which should be maximized. To achieve this, we aim to maximize the difference between T_c and T_h, while minimizing M_c. However, in a hypothetical scenario with $M_c = 5$ g, $M_h = 495$ g, $T_c = 273$K, $T_h = 373K$, and $E = 6.58$ g, the uncertainty σ_E associated with E is equal to 2.6 g, which is approximately $\frac{1}{3}$ of the value of E. Realistically, this experiment is challenging to conduct, primarily because it would be extremely difficult to maintain thermal equilibrium for 5 g of water with the internal wall.

A possible mitigation of this problem, it is to use hot water and ice instead of water at different temperatures.

For the ice-water case, the heat-balance equation to retrieve E becomes:

$$\underbrace{Q_{hot\ water}}_{M_h C(T_f - T_h)} + \underbrace{Q_{Container}}_{M_c C_c (T_f - T_h)} + \underbrace{Q_{melting\ ice}}_{LM_i} + \underbrace{Q_{cold\ water}}_{M_i C(T_f - T_c)} = 0 \tag{A9}$$

From where we can derive E as follow:

$$E = \frac{M_i(C_i T_i - L - T_f)}{C(T_f - T_h)} - M_h \tag{A10}$$

Here, M_i and T_i represent the mass and temperature of ice, while M_h and T_h represent the mass and temperature of hot water.

Also for this case we can propagate the measurements uncertainty and find the associated σ_E

$$\sigma_E = \sqrt{\left(\frac{\partial E}{\partial M_i}\right)^2 \sigma_{M_i}^2 + \left(\frac{\partial E}{\partial M_h}\right)^2 \sigma_{M_h}^2 + \left(\frac{\partial E}{\partial T_h}\right)^2 \sigma_{T_h}^2 + \left(\frac{\partial E}{\partial T_f}\right)^2 \sigma_{T_f}^2 + \left(\frac{\partial E}{\partial T_i}\right)^2 \sigma_{T_i}^2} \tag{A11}$$

The partial derivatives in Eq. (A11) are calculated as follows:

$$\frac{\partial E}{\partial M_i} = \frac{C_i Ti - L - CT_f}{C(T_f - T_h)} \tag{A12}$$

$$\frac{\partial E}{\partial M_h} = -1 \tag{A13}$$

https://doi.org/10.5194/egusphere-2023-2892
Preprint. Discussion started: 2 January 2024

$$\frac{\partial E}{\partial T_h} = \frac{M_i(C_i Ti - L - CT_f)}{C(T_f - T_w)^2} \tag{A14}$$

$$\frac{\partial E}{\partial T_f} = \frac{-CM_i(T_f - T_h) - M_i(C_i T_i - L - CT_f)}{C(T_f - T_w)^2} \tag{A15}$$

$$\frac{\partial E}{\partial T_i} = \frac{M_i C_i}{C(T_f - T_w)} \tag{A16}$$

Analyzing the error for this case, we observe that it is strongly influenced by the difference between T_f and T_h. In a hypothetical scenario with $M_h = 300g$, $M_i = 200g$, $T_h = 373K$, $T_i = 244.5K$, and $E = 6.58g$, the uncertainty σ_E associated with E is equal to 1.6 g, which is approximately $\frac{1}{4}$ of the value of E. This is still an high uncertainty, but unlike the water-water case, this experiment does not suffer from the same limitations. Hence, if it is impossible to retrieve the exact mass and specific heat of the calorimeter, the best way to estimate E would be using hot water and ice. It is important to note that for both cases, using ice and water at extreme temperatures would lead to noticeable heat dispersion in a short amount of time, making it challenging to obtain exact temperature measurements.

Because of these reasons we destructively analyzed our calorimeters to estimate E using Eq. (5). Fortunatly this process has to be done once, and other users can use E provided in the paper i.e., $E = 6.58$g.

Appendix B

In this Appendix, we will show all the formulations partly presented in (Colbeck, 1978) that allows us to prove that the relative uncertainty produced by the melting calorimeter on the estimation of the ice volume is one order of magnitude lower than the relative uncertainty produced by the freezing calorimeter on the water volume.

We compute the relative uncertainty produced by the melting calorimeter on the estimation of the ice volume starting from Eq. (2) in the main paper, written in terms of V_i:

$$V_i = \frac{C}{\rho_i L}[M_w(T_w - T_f) - M_s(T_f - T_s)] \tag{B1}$$

Hence, we compute the partial derivatives for each of the measured variables, by assuming $k = \frac{C}{L}$:

$$\begin{cases} \frac{\partial V_i}{\partial T_w} = \frac{k}{\rho_i} M_w \\ \frac{\partial V_i}{\partial T_f} = -\frac{k}{\rho_i}(M_w + M_s) \\ \frac{\partial V_i}{\partial M_w} = \frac{k}{\rho_i}(T_w - T_f) \\ \frac{\partial V_i}{\partial M_s} = -\frac{k}{\rho_i}(T_f - T_s) \end{cases} \tag{B2}$$

https://doi.org/10.5194/egusphere-2023-2892
Preprint. Discussion started: 2 January 2024

Table B1. Variable values used for the computation of the relative uncertainty produced by the melting calorimeter on the estimation of the ice volume.

Variable	Value	Unit
C	$4.2 \cdot 10^3$	J kg^{-1}K^{-1}
L	$3.34 \cdot 10^5$	J kg^{-1}
ρ_i	917	kg m^3
M_w	1.067	kg
T_w	313.15	K
T_f	277.04	K
M_s	0.5335	kg
T_s	273.15	K

and calculate the relative uncertainty Σ_{V_i} as sum of each term:

$$\Sigma_{V_i} = \left|\frac{\partial V_i}{\partial T_w}\right|\left|\frac{T_w}{V_i}\right|\left|\frac{dT}{T_w}\right| + \left|\frac{\partial V_i}{\partial T_f}\right|\left|\frac{T_f}{V_i}\right|\left|\frac{dT}{T_f}\right| + \left|\frac{\partial V_i}{\partial M_w}\right|\left|\frac{M_w}{V_i}\right|\left|\frac{dT}{M_w}\right| + \left|\frac{\partial V_i}{\partial M_s}\right|\left|\frac{M_s}{V_i}\right|\left|\frac{dT}{M_s}\right| \tag{B3}$$

By simplifying, we obtain:

$$\Sigma_{V_i} = \left|\frac{\partial V_i}{\partial T_w}\right|\left|\frac{dT}{V_i}\right| + \left|\frac{\partial V_i}{\partial T_f}\right|\left|\frac{dT}{V_i}\right| + \left|\frac{\partial V_i}{\partial M_w}\right|\left|\frac{dM}{V_i}\right| + \left|\frac{\partial V_i}{\partial M_s}\right|\left|\frac{dM}{V_i}\right| \tag{B4}$$

By considering the values reported in Table B1, we obtain $\Sigma_{V_i} = 0.007426\text{Kg}$. The values in the table are obtained by considering a snow sample with $M_w = 2 \cdot M_s$, $V_s = 10^{-3}\text{m}^3$, $V_i = 500 \cdot 10^{-6}\text{m}^3$, $V_i = 75 \cdot 10^{-6}\text{m}^3$ and $V_a = 425 \cdot 10^{-6}\text{m}^3$.

Similarly, for the freeezing calorimeter we can compute the relative uncertainty on the estimation of the water volume starting from the equation of Jones, Eq. (4) in the main paper, written in terms of V_W:

$$V_w = \frac{M_o C_o (T_{fo} - T_o) + M_s C_s (T_{fo} - T_s)}{\rho_w L} \tag{B5}$$

Hence, we compute the partial derivatives for each of the measured variables, by assuming $k = \frac{C}{L}$:

$$\begin{cases} \dfrac{\partial V_w}{\partial T_o} = -\dfrac{M_o C_o}{\rho_w L} \\ \dfrac{\partial V_w}{\partial T_{fo}} = \dfrac{M_o C_o + M_s C_s}{\rho_w L} \\ \dfrac{\partial V_w}{\partial M_o} = \dfrac{C_o (T_{fo} - T_o)}{\rho_w L} \\ \dfrac{\partial V_w}{\partial M_s} = \dfrac{C_s (T_{fo} - T_s)}{\rho_w L} \end{cases} \tag{B6}$$

and calculate the relative uncertainty Σ_{V_w} as sum of each term:

https://doi.org/10.5194/egusphere-2023-2892
Preprint. Discussion started: 2 January 2024

Table B2. Variable values used for the computation of the relative uncertainty produced by the freezing calorimeter on the estimation of the water volume.

Variable	Value	Unit
C_o	$1.83 \cdot 10^3$	J kg^{-1}K^{-1}
C_s	$2.09 \cdot 10^3$	J kg^{-1}K^{-1}
L	$3.34 \cdot 10^5$	J kg^{-1}
ρ_w	1000	kg m^3
M_o	0.69355	kg
T_o	243.15	K
T_fo	267.69	K
M_s	0.5335	kg
T_s	273.15	K

$$\Sigma_{V_w} = \left|\frac{\partial V_w}{\partial T_o}\right|\left|\frac{T_o}{V_w}\right|\left|\frac{dT}{T_o}\right| + \left|\frac{\partial V_w}{\partial T_{fo}}\right|\left|\frac{T_{fo}}{V_w}\right|\left|\frac{dT}{T_{fo}}\right| + \left|\frac{\partial V_w}{\partial M_o}\right|\left|\frac{M_o}{V_w}\right|\left|\frac{dM}{M_o}\right| + \left|\frac{\partial V_w}{\partial M_s}\right|\left|\frac{M_s}{V_w}\right|\left|\frac{dM}{M_s}\right| \tag{B7}$$

By simplifying, we obtain:

$$\Sigma_{V_w} = \left|\frac{\partial V_w}{\partial T_o}\right|\left|\frac{dT}{V_w}\right| + \left|\frac{\partial V_w}{\partial T_{fo}}\right|\left|\frac{dT}{V_w}\right| + \left|\frac{\partial V_w}{\partial M_o}\right|\left|\frac{dM}{V_w}\right| + \left|\frac{\partial V_w}{\partial M_s}\right|\left|\frac{dM}{V_w}\right| \tag{B8}$$

dM and dT are the instrumental uncertainties and are fixed to 10^{-4} g and 0.1 K respectively. By considering the values reported in Table B2, we obtain $\Sigma_{V_w} = 0.014809\text{Kg}$ that results twice the error Σ_{V_i} calculated for the melting calorimeter. The values in the table are obtained by considering a snow sample with $M_o = 1.3 \cdot M_s$, $V_s = 10^{-3}\text{m}^3$, $V_i = 500 \cdot 10^{-6}\text{m}^3$, $V_i = 75 \cdot 10^{-6}\text{m}^3$ and $V_a = 425 \cdot 10^{-6}\text{m}^3$.

Author contributions. RB and CM designed the research, carried out the experiments, processed the data, and wrote the paper; VP helped with the mathematical formulation and wrote the Appendix with the relative codes; NC contributed with the field experiments;MB and FC contributed to the WFJ data collection; all the authors contributed to the analysis and interpretation of the results and provided feedback on the final text.

Competing interests. The authors declare that they have no conflict of interest.

Acknowledgements. This work was supported by the joint project Swiss National Science Foundation (SNF) - Autonomous Province of Bolzano (Italy) "Snowtinel: Sentinel-1 SAR assisted catchment hydrology: toward an improved snow-melt dynamics for alpine regions" Contract No. 200021L205190.

https://doi.org/10.5194/egusphere-2023-2892
Preprint. Discussion started: 2 January 2024

References

Austin, R. T.: Determination of the liquid water content of snow by freezing calorimetry, Tech. rep., 1990.

Avanzi, F., Petrucci, G., Matzl, M., Schneebeli, M., and De Michele, C.: Early formation of preferential flow in a homogeneous snowpack observed by micro-CT, Water Resources Research, 53, 3713–3729, https://doi.org/https://doi.org/10.1002/2016WR019502, 2017.

Boyne, H. and Fisk, D.: A comparison of snow cover liquid water measurement techniques, Water Resources Research, 23, 1833–1836, 1987.

Colbeck, S.: The difficulties of measuring the water saturation and porosity of snow, Journal of Glaciology, 20, 189–201, 1978.

Denoth, A. and Foglar, A.: Recent developments of snow moisture dielectric devices, in: Proceedings of the InteTllational Snow Science Workshop, Lake Ta/we, CA, pp. 22–25, 1986.

Fasani, D., Cernuschi, F., and Colombo, L.: Calorimetric determination of wet snow liquid water content: The effect of test conditions on the calorimeter constant and its impact on the measurement uncertainty, Cold Regions Science and Technology, 214, 103 959, https://doi.org/https://doi.org/10.1016/j.coldregions.2023.103959, 2023.

Fisk, D.: Method of Measuring Liquid Water Mass Fraction of Snow by Alcohol Solution, Journal of Glaciology, 32, 538–539, https://doi.org/10.3189/S0022143000012272, 1986.

FPGA Company: SLF Snow Sensor, https://fpga-company.com/wp-content/uploads/2023/01/InfraSnow-User-Manual-Version-1.01.pdf.

Gagliano, E., Shean, D., Henderson, S., and Vanderwilt, S.: Capturing the Onset of Mountain Snowmelt Runoff Using Satellite Synthetic Aperture Radar, Geophysical Research Letters, 50, e2023GL105 303, https://doi.org/https://doi.org/10.1029/2023GL105303, e2023GL105303 2023GL105303, 2023.

Hirashima, H., Avanzi, F., and Wever, N.: Wet-Snow Metamorphism Drives the Transition From Preferential to Matrix Flow in Snow, Geophysical Research Letters, 46, 14 548–14 557, https://doi.org/https://doi.org/10.1029/2019GL084152, 2019.

Ice: The international classification for seasonal snow on the ground, https://api.semanticscholar.org/CorpusID:127514739, 1990.

Jones, E. B., Rango, A., and Howell, S. M.: Snowpack Liquid Water Determinations Using Freezing Calorimetry, Hydrology Research, 14, 113–126, https://doi.org/10.2166/nh.1983.0010, 1983.

Jones, R. N.: Comparison of centrifuge and freezing calorimeter methods for measuring free water in snow, NASA STI/Recon Technical Report N, 80, 13 319, 1979.

Kawashima, K., Endo, T., and Takeuchi, Y.: A portable calorimeter for measuring liquid-water content of wet snow, Annals of Glaciology, 26, 103–106, https://doi.org/10.3189/1998AoG26-1-103-106, 1998.

Kinar, N. J. and Pomeroy, J. W.: Measurement of the physical properties of the snowpack, Reviews of Geophysics, 53, 481–544, https://doi.org/https://doi.org/10.1002/2015RG000481, 2015.

Linlor, W. I., C. F. D. M. M. F. S. J. L.: Snow wetness measurements for melt forecasting, in: Operational Appl. of Satellite Snowcover Observations, vol. 1, p. 375, 1975.

Marin, C., Bertoldi, G., Premier, V., Callegari, M., Brida, C., Hürkamp, K., Tschiersch, J., Zebisch, M., and Notarnicola, C.: Use of Sentinel-1 radar observations to evaluate snowmelt dynamics in alpine regions, The Cryosphere, 14, 935–956, https://doi.org/10.5194/tc-14-935-2020, 2020.

Marty, C. and Meister, R.: Long-term snow and weather observations at Weissfluhjoch and its relation to other high-altitude observatories in the Alps, Theoretical and Applied Climatology, 110, https://doi.org/10.1007/s00704-012-0584-3, 2012.

Moffat, R. J.: Describing the uncertainties in experimental results, Experimental thermal and fluid science, 1, 3–17, 1988.

https://doi.org/10.5194/egusphere-2023-2892
Preprint. Discussion started: 2 January 2024

Proksch, M., Rutter, N., Fierz, C., and Schneebeli, M.: Intercomparison of snow density measurements: bias, precision, and vertical resolution, The Cryosphere, 10, 371–384, https://doi.org/10.5194/tc-10-371-2016, 2016.

Techel, F. and Pielmeier, C.: Point observations of liquid water content in wet snow; investigating methodical, spatial and temporal aspects, The Cryosphere, 5, 405–418, https://doi.org/10.5194/tc-5-405-2011, 2011.

Wever, N., Fierz, C., Mitterer, C., Hirashima, H., and Lehning, M.: Solving Richards Equation for snow improves snowpack meltwater runoff estimations in detailed multi-layer snowpack model, The Cryosphere, 8, 257–274, https://doi.org/10.5194/tc-8-257-2014, 2014.

Wever, N., Vera Valero, C., and Fierz, C.: Assessing wet snow avalanche activity using detailed physics based snowpack simulations, Geophysical Research Letters, 43, 5732–5740, https://doi.org/https://doi.org/10.1002/2016GL068428, 2016.

Yosida, Z.: Instruments and Methods: A Calorimeter for Measuring the Free Water Content of Wet Snow, Journal of Glaciology, 3, 574–576, https://doi.org/10.3189/S0022143000023698, 1960.